Research on the Spectral Reconstruction of a Low-Dimensional Filter Array Micro-Spectrometer Based on a Truncated Singular Value Decomposition-Convex Optimization Algorithm

Jiakun Zhang, Liu Zhang, Ying Song, and Yan Zheng

***Abstract*—Currently, the engineering of miniature spectrometers mainly faces three problems: the mismatch between the number of filters at the front end of the detector and the spectral reconstruction accuracy; the lack of a stable spectral reconstruction algorithm; and the lack of a spectral reconstruction evaluation method suitable for engineering. Therefore, based on 20 sets of filters, this paper classifies and optimizes the filter array by the K-means algorithm and particle swarm algorithm, and obtains the optimal filter combination under different matrix dimensions. Then, the truncated singular value decomposition-convex optimization algorithm is used for high-precision spectral reconstruction.In terms of spectral evaluation, due to the strong randomness of the target detected during the working process of the spectrometer, the standard value of the target spectrum cannot be obtained. Therefore, we adopt the method of joint cross-validation of multiple sets of data for spectral evaluation. The results show that when the random error of +/− 2 code values is applied multiple times for reconstruction, the spectral angle cosine value between the reconstructed curves becomes more than 0.995, which proves that the spectral reconstruction under this algorithm has high stability. At the same time, the spectral angle cosine value of the spectral reconstruction curve and the standard curve can reach above 0.99, meaning that it realizes a high-precision spectral reconstruction effect. A high-precision spectral reconstruction algorithm based on truncated singular value-convex optimization, is established in this paper, providing important scientific research value for the engineering application of micro-spectrometers.**

***Index Terms*—Spectral reconstruction spectral analysis convex optimization cross-validation.**

I. Introduction

As AN important instrument for obtaining spectral information, spectrometers are gradually developing toward integration and miniaturization. Currently, the engineering of miniature spectrometers mainly faces three problems. The first is the mismatch between the number of filters at the front end of the detector and the spectral reconstruction accuracy; the second is the lack of a stable spectral reconstruction algorithm; and the third is the lack of a spectral reconstruction evaluation method suitable for engineering. In recent years, micro-spectrometers based on filter arrays have received extensive attention [1], [2], [3], [4], [5]. The advantage of a miniature spectrometer over a traditional spectrometer is that it does not need prisms, gratings, or other optical elements to split light [6], [7], but through the mathematical relationship between target spectrum, filter array, detector quantum efficiency, and gray value, $\mathbf{AX} = \mathbf{B}$ is calculated.

The spectral reconstruction algorithm is the core of the miniature spectrometer, and its function is to solve the equation system $\mathbf{AX} = \mathbf{B}$ with high precision. Scholars engaged in related research have proposed many high-precision spectral reconstruction algorithms. However, these algorithms are often proposed under ideal conditions without considering the errors generated during the development and operation of the spectrometer. Currently, there are three main problems in the miniaturization of micro-spectrometers. First, regarding the issue of the number of filter arrays, since an increase in the number of filters will lead to high spectral reconstruction accuracy, the number of filters used in previous related studies exceeds 190 [8], [9], but this is not conducive to the miniaturization of the spectrometer. Second, regarding issues for developing a universal high-precision spectral reconstruction algorithm, the spectrometer will produce many errors in the working process, for example, the processing error of the filter array, the noise of the detector itself, and the error of the gray value of the detector. The relevant research does not truly test the error range but simply applies a random error of 80 dB∼30 dB, which is inconsistent with the real error environment. Finally, regarding the issue of the engineered spectral reconstruction evaluation criteria, the evaluations of spectral reconstructions in previous studies were all performed under the

Manuscript received 23 September 2022; revised 11 February 2023; accepted 9 March 2023. Date of publication 20 March 2023; date of current version 5 April 2023. This work was supported in part by the Foundation of Equipment Pre-research Area under Grant 6B2B5347, in part by the National Natural Science Foundation of China (NSFC) under Grant 61905243, in part by the Scientific Research Project of Education Department of Jilin Province under Grant JJKH20220992KJ, and in part by Jilin Province Science & Technology Development Program Project in China under Grant 20200401071GX. *(Corresponding author: Yan Zheng.)*

The authors are with the College of Instrumentation and Electrical Engineering, Jilin University, Changchun, Jilin 130012, China, and also with the National Engineering Research Center of Geophysics Exploration Instruments, Jilin University, Changchun 130061, China (e-mail: jkzhang20@mails.jlu.edu.cn; zhangliu@jlu.edu.cn; songyingtec@126.com; zhengyan19@mails.jlu.edu.cn).

Digital Object Identifier 10.1109/JPHOT.2023.3256561

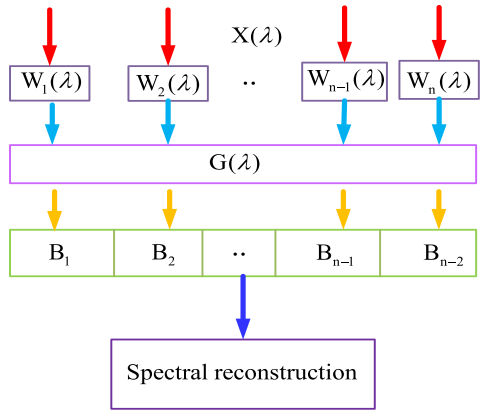

Fig. 1. Schematic of proposed micro-spectrometer.

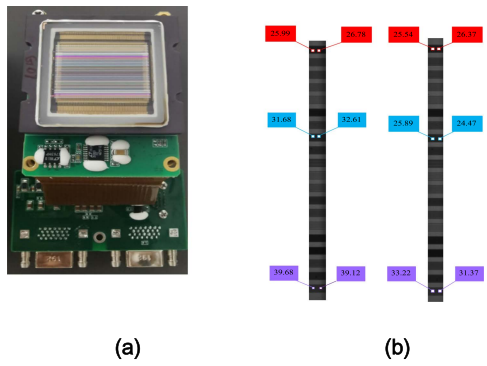

Fig. 2. (a) Schematic diagram of the micro-spectrometer filter array; (b) Grayscale image.

assumption of known targets. In practice, the objects observed in the working process of the miniature spectrometer have high randomness, and we cannot obtain the true curve of the spectrum in advance. Therefore, it is necessary to perform a reconstruction evaluation on the reconstructed spectrum under the condition of an unknown target, and thus, a high-precision and stable spectral reconstruction algorithm suitable for engineering is needed. Based on the above three observations, first, on the basis of 20 filter pairs, the optimal filter combination is selected by the K-means algorithm and particle swarm optimization algorithm, then the truncated singular value decomposition-convex optimization (Cvx) algorithm is used to reconstruct the spectrum, and finally, a spectral evaluation is conducted according to the multigroup cross-validation method, which satisfies the engineering requirements. Therefore, for the first time, we apply joint cross-validation of multiple sets of data for spectral evaluation. The results show that when the random error of +/− 2 code values is applied multiple times for reconstruction, the spectral angle cosine between the reconstructed curves exceeds 0.995, which proves that the spectral reconstruction under this algorithm has high stability. At the same time, the spectral angle cosines of the spectral reconstruction curve and the standard curve can exceed 0.99, thus achieving a high-precision spectral reconstruction effect. A high-precision truncated singular value decomposition-Cvx spectral reconstruction algorithm (Tsvd-Cvx) suitable for engineering applications is established in this paper, which provides important scientific research value for the engineering application of micro-spectrometers.

II. Working Principle of Miniature Spectrometer

The working principle of the spectrometer is shown in Fig. 1. The target spectrum $\mathrm{X}(\lambda)$ passes through the filter array at the front of the detector $\mathrm{W}(\lambda)$. The gray value B [10], [11], [12] is obtained after modulation of the quantum efficiency $\mathrm{G}(\lambda)$ of the detector.

The relationship among $\mathrm{X}(\lambda)$, $\mathrm{W}(\lambda)$, and $\mathrm{G}(\lambda)$ is shown in (1).

$$\int_{\lambda_2}^{\lambda_1} W(\lambda) \cdot G(\lambda) \cdot X(\lambda) = B \tag{1}$$

Let $A(\lambda) = W(\lambda) \cdot G(\lambda)$, then (1) is simplified as (2).

$$\int_{\lambda_2}^{\lambda_1} A(\lambda) \cdot X(\lambda) = B \tag{2}$$

After discretizing (2), we can obtain (3).

$$\boldsymbol{A} \cdot \boldsymbol{X} = \boldsymbol{B} \tag{3}$$

The specific expression of (3) is shown in (4).

$$\begin{pmatrix} a_{11} & \mathbf{K} & a_{1n} \\ \mathbf{M} & \mathbf{O} & \mathbf{M} \\ a_{n1} & \mathbf{L} & a_{nn} \end{pmatrix} \cdot \begin{pmatrix} x_1 \\ \mathbf{M} \\ x_n \end{pmatrix} = \begin{pmatrix} b_1 \\ \mathbf{M} \\ b_n \end{pmatrix} \tag{4}$$

The spectral reconstruction problem of the miniature spectrometer thus becomes a problem of solving equations. The micro-spectrometer filter array is shown in Fig. 2(a). The spectral range of the micro-spectrometer for visible light is 400–900 nm, The spectral range of the micro-spectrometer for visible light is 400–900 nm, and through simulation calculations, we can use 20 groups of filters to perform spectral inversion to obtain the spectral information of the 400–900 nm target spectrum. However, the working process of the spectrometer will be affected by a variety of error sources. These error sources are divided into four categories: The first is the influence of the noise of the detector itself; the second is the influence of the optical system aberration; the third is the influence of stray light on the energy of the detector; and the fourth is the filter-processing error. The first three errors have a greater impact on the detector gray value (matrix **B**), After detection, the error experienced by the detector is about two gray values as shown in Fig. 2(b): This is far beyond the 80 dB∼30 dB error of the signal-to-noise ratio in the previous study. In the operation of the spectrometer, the above error is represented by the gray value.The methods used for (3) in previous related studies include GPSR [13], OMP [14], L2 Regularization [10] and the CNN algorithm [15]; however, these methods all have the same drawbacks. First, the number of filters required is large. The second is that they must be solved under the condition of a known target. The third is that the applied error is small in the simulation process, which does not meet the actual work requirements of the spectrometer.

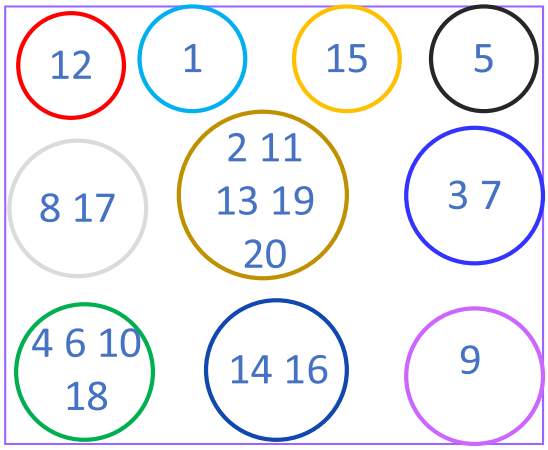

Fig. 3. K-means clustering results when number of clusters is 10.

TABLE I
FILTER COMBINATION OPTIMIZATION RESULTS

Number of clusters	Optimal filter combination	Condition number	Full rank
5	14 8 4 12 5	43.82	Yes
6	9 6 3 5 15 14	62.49	Yes
7	1 15 13 11 6 7 9	102.06	Yes
8	11 20 7 9 14 8 12 16	144.01	Yes
9	8 4 17 20 6 16 12 1 5	162.41	Yes
10	12 1 15 5 8 19 3 10 16 9	2007	Yes
12	12 14 15 6 5 10 8 7 4 9 12 1	13415	Yes
14	16 13 5 12 8 20 2 1 14 17 4 10 15 9	209843	Yes
15	5 4 13 8 20 10 17 7 9 18 19 11 1 14 15	1001439	Yes

III. Filter Optimization Selection Process

A. The Principle of Filter Selection

The analysis in the second section indicates that there is a large error in the working process of the spectrometer, which has a huge impact on the solution accuracy of (3). In fact, the excessively large size of matrix **A** in (3) is the root cause of poor solution accuracy. However, the precise solution of (3) can be improved through different filter combinations. The essence of filter combination screening is to reduce the condition number of matrix **A** under the condition of full rank of matrix **A**. The selection of filter array combinations is based on (5) [16], [17] and (6) [18]. (5) calculates the cosine of the angle between the two curves, and its purpose is to judge the similarity of the two curves. A larger $\cos\theta$ value implies that the curves are more similar. The purpose of (5) is to ensure the full rank of the **A** matrix and the uniqueness of the solution of (3). Terms x_i and y_i represent discrete points at wavelengths of the two spectral curves. (6) is the definition of matrix condition number, and the condition number can be determined by the ratio of the largest eigenvalue ($\sigma_{\max}$) to the smallest eigenvalue ($\sigma_{\min}$). A larger condition number leads to a more ill-conditioned matrix.

$$\cos\theta = \frac{\sum_{i=1}^{n} x_i y_i}{\sqrt{\sum_{i=1}^{n} x_i^2} \cdot \sqrt{\sum_{i=1}^{n} y_i^2}} \tag{5}$$

$$Cond(\boldsymbol{A}) = \frac{\sigma_{\max}}{\sigma_{\min}} \tag{6}$$

B. K-Means Filter Clustering and Optimization

First, 20 A(λ) are numbered including the multiplication of the detector quantum efficiency curve and the filter transmittance curve (20 A(λ) curves are given in the Appendix). The K-means algorithm was used to cluster 20 filters based on (5). In each cluster, the similarity between A(λ) is high, and the similarity in different A(λ) clusters is low. For example, Fig. 3 shows the clustering result with 10 clusters; each circle represents the filter number.

After the clustering is completed, (6) is used as the evaluation function, and the particle swarm optimization algorithm is used for optimization to find the minimum condition number. The optimization results are shown in Table I.

Table I shows that the matrices are all full rank after the filter is selected, and the matrix condition number becomes larger and larger an increase in the number of clusters. In turn, the ill-conditioned degree of the matrix becomes higher and higher, which is very unfavorable for an (3) solution. It is necessary to make full use of the optimization results in Table I for spectral reconstruction on the basis of filter combinations with smaller condition numbers.

IV. Spectral Reconstruction Algorithms

A. Truncated Singular Value Decomposition (Tsvd)

Truncated singular value decomposition [19], [20] is a classic method for dealing with large condition number matrices. After the matrix undergoes singular value decomposition, a set of Singular values matrices arranged from large to small are generated as shown in (7) and (8) ($\sigma_1 > \sigma_2 > \mathbf{LL} > \sigma_{\mathbf{n}}$). The minimum value of these singular values is often very small, and these smaller singular values are the main factors affecting the larger condition number of the matrix. Relatively large singular values represent more reliable parts, and smaller singular values represent large floating and unreliable parts. Therefore, our most direct approach is to "truncate" the singular values matrix and discard the smaller part of the singular values matrix to reduce the condition number of the matrix.

$$\boldsymbol{A} = \boldsymbol{U}\boldsymbol{D}\boldsymbol{V}^T \tag{7}$$

$$\boldsymbol{D} = diag(\sigma_1, \sigma_2, \mathbf{L}, \sigma_{\mathbf{n}}) \tag{8}$$

When the singular values are not "truncated," (3) is shown as (9).

$$\boldsymbol{X} = \sum_{i=1}^{n} \sigma_i^{-1} v_i u_i^T \mathbf{B} \tag{9}$$

However, in order to make the solution more accurate, this paper first improves **D** according to (10), which will somewhat

reduce the condition number of matrix **A**.

$$\boldsymbol{D} = \boldsymbol{D} + \frac{\min(\boldsymbol{D})}{\boldsymbol{D}} \tag{10}$$

When "truncation" is performed on the singular values, the first t singular values are retained, and t is also called the "truncation threshold." The solution of (3) at this time is shown in (11). σ_i' is the singular value after correction.

$$\mathbf{X} = \sum_{i=1}^{t} (\sigma_i'^{-1}) v_i u_i^T \boldsymbol{B} \tag{11}$$

B. Convex Optimization

Equation (3) is a typical convex problem. Cvx [21], [22], [23] is a common method for solving (3). The general form of Cvx is shown in (12).

$$\begin{array}{ll} \text{minimize} & f_0(x) \\ \text{subject to} & f_i(x) \le 0, i = 1,2,\boldsymbol{L},m \\ & h_i(x) = 0, i = 1,2,\boldsymbol{L},n \end{array} \tag{12}$$

In (12), $f_0(x)$ is the objective function, $f_i(x)$ is the inequality constraint, and $h_i(x)$ is the equality constraint. The Cvx problem becomes a linear programming problem when the objective function and constraint function of Cvx are both affine functions. (12) indicates that the Cvx can obtain more accurate results with appropriate constraints, but the constraints are very important to the solution.

C. Spectral Reconstruction Based on Tsvd and Cvx (Tsvd-Cvx)

Although Tsvd and Cvx can each obtain relatively accurate results, they each also have their own shortcomings. Tsvd has two disadvantages: The first is that the discrete values solved may have negative values, and the second is that when the condition number is too large, too much spectral information needs to be lost to obtain a lower condition number. The solution method of Cvx is more flexible, and different solutions can be obtained by adding different constraints. However, the constraints are critical to obtaining an accurate solution. If the constraints are insufficient, then discrete values with large deviations from the standard value will be obtained. In order to obtain a high-precision reconstruction curve, this paper combines the two algorithms, and takes the result obtained by the Tsvd algorithm as the constraint of the Cvx algorithm to reconstruct two typical spectral curves.

First, an error of three thousandths is applied to matrix **A**, and a random error of plus or minus three gray values is applied to matrix **B**. According to the results obtained from the filter combination optimization in Table I, the discrete values with the cluster numbers 5, 6, and 7 are first solved by truncated singular value decomposition.

Tables II–IV show that the number of discrete points is small although the three sets of results calculated by truncating singular values have high precision. Taking the calculation result of the cluster class as 5, the wavelengths corresponding to these five discrete points are 450 nm, 550 nm, 650 nm, 750 nm, and 850 nm.

TABLE II
NUMBER OF CLUSTERS IS 5 (TARGET 1)

Discrete values	Standard value	Error
0.4280	0.4603	−0.0323
0.4866	0.5275	−0.0409
0.5204	0.4792	0.4127
0.5275	0.5088	0.0187
0.5275	0.5284	−0.0009

TABLE III
NUMBER OF CLUSTERS IS 6 (TARGET 1)

Discrete values	Standard value	Error
0.4099	0.4497	−0.0397
0.5460	0.5295	0.0165
0.4565	0.4967	−0.0402
0.5007	0.4799	0.0208
0.5610	0.5220	0.0390
0.5551	0.5273	0.2784

TABLE IV
NUMBER OF CLUSTERS IS 7 (TARGET 1)

Discrete values	Standard value	Error
0.4806	0.4422	0.0384
0.5390	0.5224	0.0167
0.4700	0.5175	−0.0475
0.4627	0.4764	−0.0137
0.5364	0.4911	0.0452
0.5680	0.5305	0.0375
0.5003	0.5257	−0.0255

When fitting these five points in the range of 400–900 nm, there may be points that are quite different from the standard values because there are no discrete points in the range of 400–450 nm and 850–900 nm. Thus, upon adding two discrete points of 400 nm and 425 nm in the range of 400–450 nm, the value of these two discrete points is equal to the discrete value at 450 nm. Similarly, upon adding two discrete points of 850 nm and 900 nm in the range of 850–900 nm, these two discrete points have a value equal to the discrete value at 875 nm. The fitting results are shown in Fig. 4.

The above three results are added to the Cvx as constraints, and the Cvx expression is shown in (13).

$$\begin{array}{ll} \text{minimize} & ||\mathbf{AX} - \mathbf{B}||_2 \\ \text{subject to} & |X_i - X_{i+1}| < R, i = 1,2,\boldsymbol{L},n-1 \\ & |\frac{X_i + X_{i+1}}{2} - Y_j| < T \\ & X_i < \max(Y) \\ & X_i > \min(Y) \\ & i = 1,3,\boldsymbol{L},n; j = 1,2,\boldsymbol{L}\frac{n}{2} \end{array} \tag{13}$$

In (13), $|X_i - X_{i+1}| < R$ is the constraint of two adjacent discrete points, $|X_i - mean| < T$ is the constraint between each discrete point and the target mean, $|\frac{X_i + X_{i+1}}{2} - Y_j| < T$ is the constraint of truncated singular value decomposition, and Y_j is the result of truncated singular value calculation.

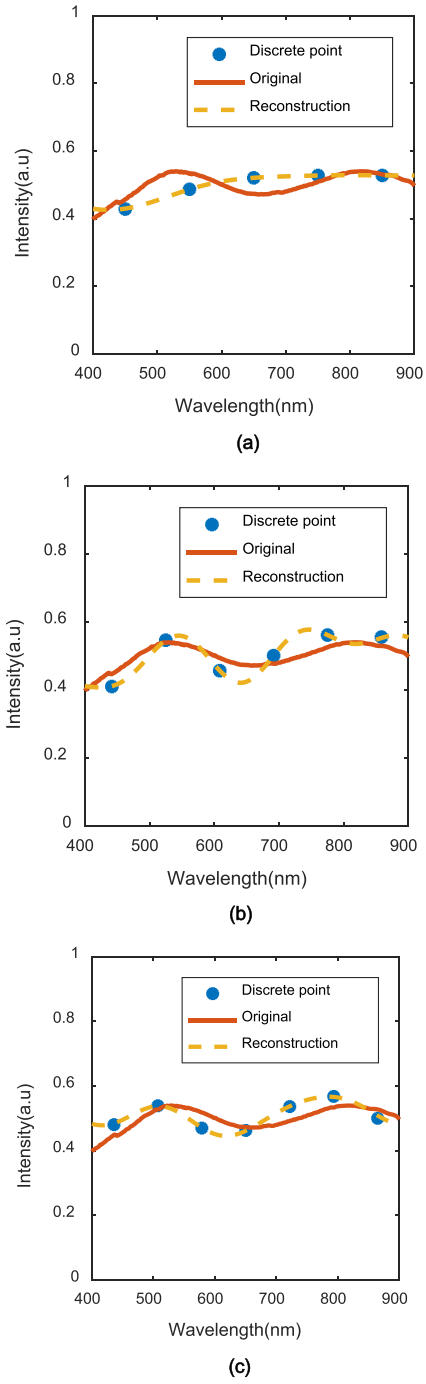

Fig. 4. Calculation results of Tsvd: (a) Number of clusters is 5, (b) Number of clusters is 6, and (c) Number of clusters is 7.

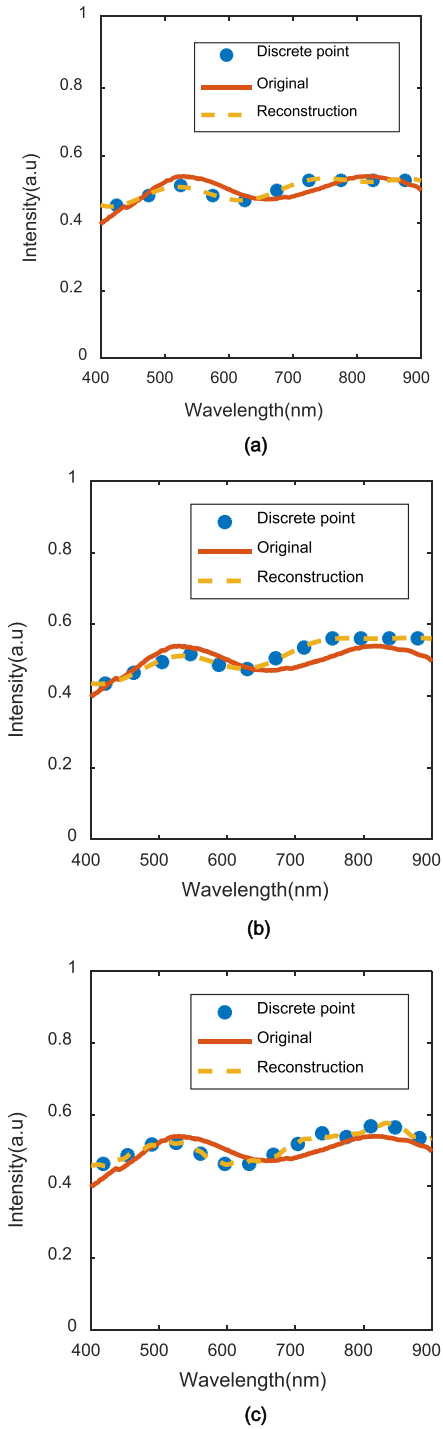

Fig. 5. Calculation results of Tsvd constrained Cvx, (a) Number of clusters is 10, (b) Number of clusters is 12, and (c) Number of clusters is 14.

Terms $X_i < \max(Y)$ and $X_i > \min(Y)$ are boundary constraints, which determine the solution range of CVX. Solving discrete values and fitting spectral curves are shown in Fig. 5.

The above simulation is aimed at the reconstruction result of the relatively flat spectral curve. To verify the universality of the algorithm, the reconstruction is performed on the spectral curve with obvious peaks (target 2). Similarly, we first applied an error of three thousandths to matrix **A**, and then applied a random error of plus or minus 3 grayscale values to matrix **B**. The truncated singular value decomposition results are shown in Tables V–VII.

Upon fitting the discrete points in Tables V–VII, we get the results in Fig. 6.

TABLE V
NUMBER OF CLUSTERS IS 5 (TARGET 2)

Discrete values	Standard value	Error
0.3728	0.3207	0.0528
0.3401	0.3937	−0.0536
0.2191	0.2569	−0.0377
0.1976	0.1976	0
0.2570	0.2113	0.4566

TABLE VI
NUMBER OF CLUSTERS IS 6 (TARGET 2)

Discrete values	Standard value	Error
0.2049	0.3089	−0.1040
0.4485	0.3972	0.0513
0.2675	0.3299	−0.0624
0.2740	0.2087	0.0652
0.2691	0.2010	0.0681
0.1935	0.2118	−0.0182

TABLE VII
NUMBER OF CLUSTERS IS 7 (TARGET 2)

Discrete values	Standard value	Error
0.3193	0.3009	0.0184
0.4172	0.3880	0.0292
0.3287	0.3786	−0.0500
0.2842	0.2548	0.0295
0.2633	0.1959	0.0674
0.1639	0.2046	−0.0408
0.1601	0.2120	−0.0519

The Cvx solution is performed upon taking the Tsvd result as a constraint (Fig. 7).

V. SPECTRAL CURVE EVALUATION

The previously studied evaluation functions include MSE, ARE, and RE. The specific table expressions are shown in (14), (15), and (16); here, y_i is the standard value, and $\hat{y}$ is the reconstructed value.

$$ARE = \frac{||y_i - \hat{y}||_2^2}{||y_i||_2^2} \tag{14}$$

$$RE = \frac{||y_i - \hat{y}||_2}{||y_i||_2} \tag{15}$$

$$MSE = \frac{1}{n}\sum_{k=1}^{n}(y_i - \hat{y})^2 \tag{16}$$

These evaluation methods are established under the condition of a known target spectrum. The target of the spectrometer is random in the working process, and the standard value of the target spectrum is unknown; thus, the above evaluation criteria are not applicable as the evaluation criteria for the reconstruction accuracy of the target spectrum. This paper proposes a cross-validation method to solve this problem. The three same target spectral curves obtained by fitting the cluster numbers of 10, 12, and 14 were evaluated with each other, and the spectral angle cosine value ($\cos\theta$) between the three curves was calculated. The calculation results are shown in Table VIII.

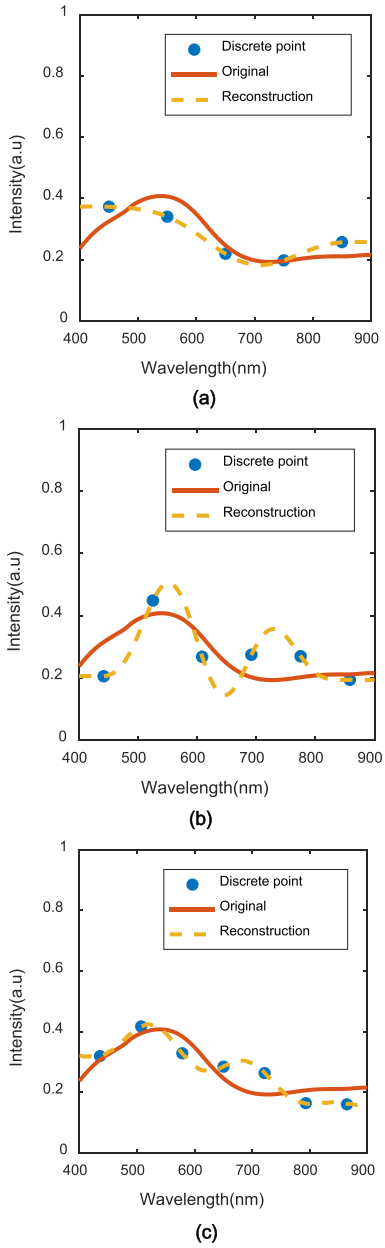

Fig. 6. Calculation results of Tsvd: (a) Number of clusters is 5, (b) Number of clusters is 6, and (c) Number of clusters is 7.

TABLE VIII
CALCULATION RESULTS OF $\cos\theta$ THE RECONSTRUCTED CURVE (TARGET 1)

Number of clusters	$\cos\theta$
10 and 14	0.9994
10 and 12	0.9995
12 and 14	0.9996

Table VIII shows that $\cos\theta$ values between the three reconstruction curves of target 1 are very close, and the final reconstruction curve can be obtained by averaging the three reconstruction curves in Fig. 4 as shown in Fig. 8(a).

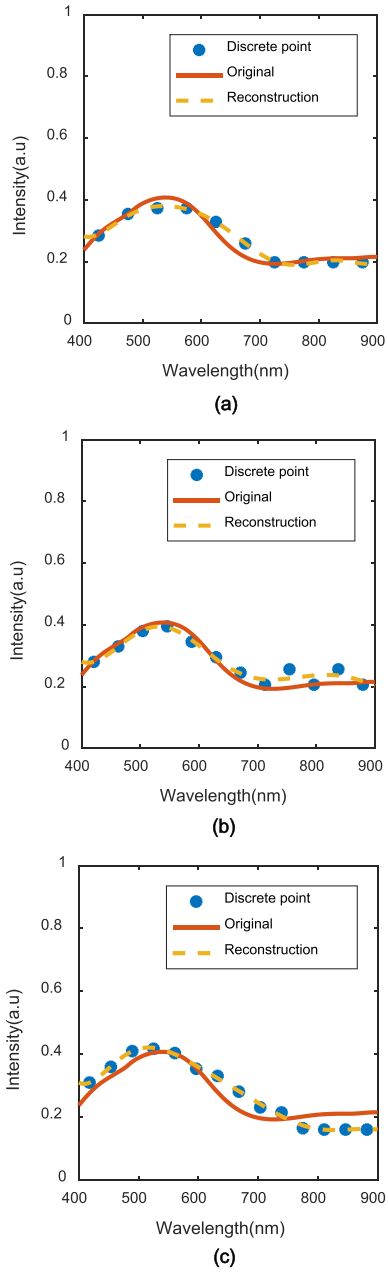

Fig. 7. Calculation results of Tsvd constrained Cvx: (a) Number of clusters is 10, (b) Number of clusters is 12, and (c) Number of clusters is 14.

Table IX shows that the $\cos\theta$ values of the three groups are significantly different; thus, the reconstruction curve can be obtained by averaging the combination with the highest spectral angle cosine value as shown in Fig. 8(b).

VI. Stability Verification

To verify the stability of the algorithm, 10 random errors are applied to (3), and the above steps are repeated to reconstruct the spectrum for stability verification of the reconstructed curve, as shown in Fig. 9.

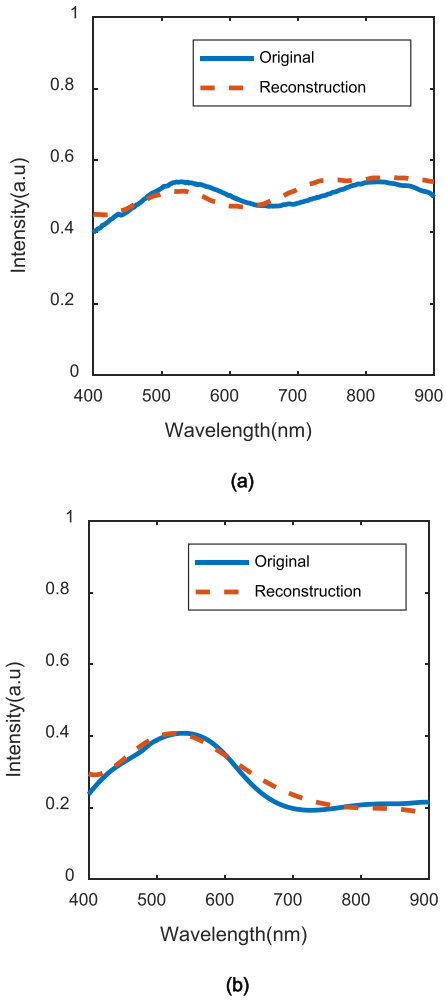

Fig. 8. Spectral reconstruction results: (a) Target 1 and (b) Target 2.

TABLE IX
Calculation Results of $\cos\theta$ the Reconstructed Curve (Target 2)

Number of clusters	$\cos\theta$
10 and 12	0.9968
10 and 14	0.9959
12 and 14	0.9891

The 10 reconstructed curves are now matched with the reconstructed curves in Fig. 8(a) (cross-validation), and the $\cos\theta$ values are obtained as shown in Table X. It can be seen from Table X that the $\cos\theta$ values of the reconstructed curves in Figs. 8(a) and 9 reach above 0.995. It can achieve a better reconstruction effect and has strong stability.

In the same way as the above operation, 10 reconstructed curves about target 2 are obtained, as shown in Fig. 10. The $\cos\theta$ values of the curves in Figs. 8(b) and 10 are shown in Table XII. All of the values reach above 0.992. The results show that the Tsvd-Cvx algorithm proposed in this paper can also achieve a better reconstruction effect for a target spectral curve with obvious convexity.

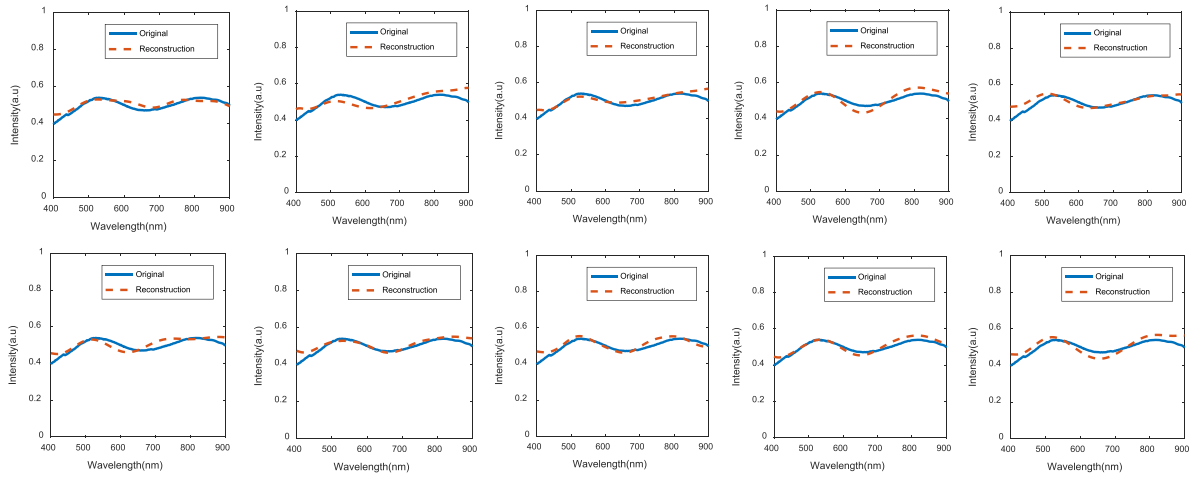

Fig. 9. Reconstructed curve after adding 10 random errors (target 1).

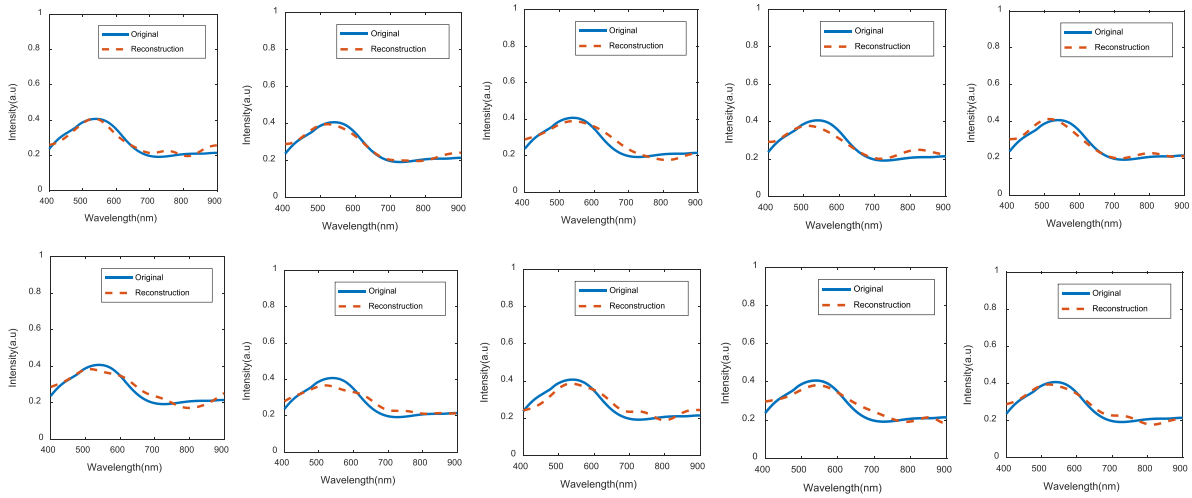

Fig. 10. Reconstructed curve after adding 10 random errors (target 2).

TABLE X
CALCULATED $\cos\theta$ VALUES FOR THE RECONSTRUCTED CURVE (TARGET 1)

Number	$\cos\theta$
1	0.9987
2	0.9998
3	0.9997
4	0.9992
5	0.9996
6	0.9988
7	0.9986
8	0.9993
9	0.9988
10	0.9982

TABLE XI
CALCULATED $\cos\theta$ VALUES FOR THE RECONSTRUCTED CURVE (TARGET 2)

Number	$\cos\theta$
1	0.9960
2	0.9981
3	0.9970
4	0.9976
5	0.9986
6	0.9951
7	0.9941
8	0.9988
9	0.9968
10	0.9994

To further test the advantages of spectral reconstruction by the proposed algorithm (Tsvd-Cvx), we compare it with the standard regularization algorithm, take the reconstructed curve obtained by the Tsvd-Cvx algorithm as a known target, analyze the similarity of the reconstructed spectral curve obtained by the standard regularization algorithm, and calculate the spectral angle cosine values of the two. The reconstruction results are shown in Fig. 11. To ensure the stability of the algorithm, 100 random errors are applied to the B value, and the mean value of the spectral angle cosine is calculated under $+/-0.01$, $+/-0.1$

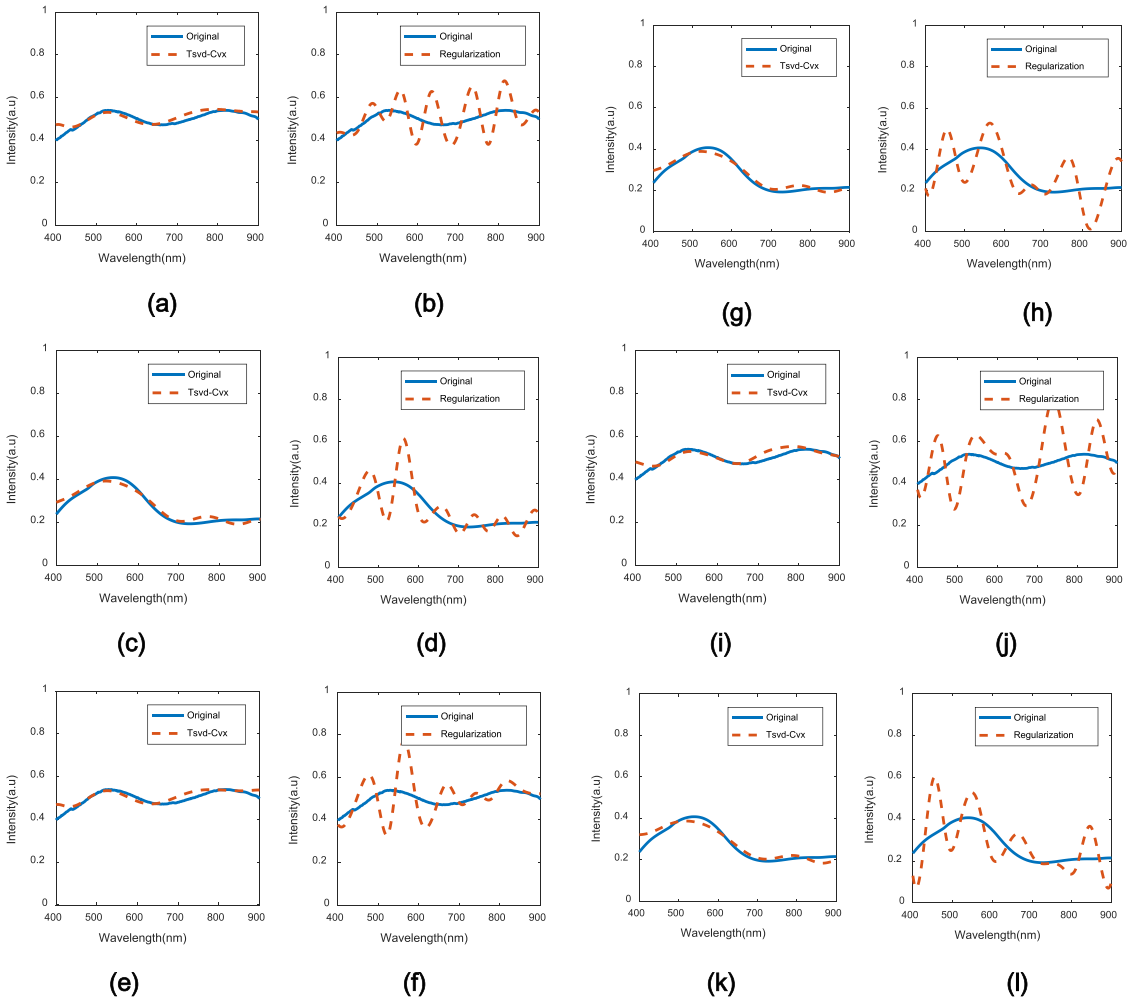

Fig. 11. Spectral reconstruction results of Tsvd-Cvx and the standard regularization algorithm under +/−0.01, +/−0.1 and +/−1 gray value error conditions. Comparison of the Tsvd-Cvx and regularization algorithms with 0.01 gray value errors: (a), (b), (c), (d). Comparison of the Tsvd-Cvx and regularization algorithms with +/−0.1 gray value errors: (e), (f), (g), (h). Comparison of the Tsvd-Cvx and regularization algorithms with +/−1 gray value errors: (i), (j), (k), (l).

TABLE XII
REGULARIZED RECONSTRUCTED SPECTRAL CURVE AND TSVD-CVX RECONSTRUCTED SPECTRAL CURVE SPECTRAL ANGLE COSINE VALUES

	Target	$\cos\theta$	Mean value of 100 times $\cos\theta$
0.01 gray value error	target 1	0.9891	0.9849
	target 2	0.9679	0.9830
0.1 gray value error	target 1	0.9856	0.9806
	target 2	0.9479	0.9633
1 gray value error	target 1	0.9712	0.8775
	target 2	0.9409	0.9120

and +/−1 gray value error environments. The results are shown in Table XII.

It can be seen from Fig. 11 and Table XII that under the condition of a gray value error of +/−0.01, the cosine value of the spectral angle reconstructed by the regularization algorithm and Tsvd-Cvx algorithm is less than 0.989, and the mean value is less than 0.985 after 100 random errors are applied, with local distortion of the spectral curve reconstructed by the regularization algorithm. Under the condition that the gray value error is +/−0.1, the spectral curve reconstructed by the regularization algorithm and the spectral curve reconstructed by the Tsvd-Cvx algorithm have cosines of less than 0.986, and 100 random errors are applied, with a mean value less than 0.981. The degree of local deformation of the spectral curve reconstructed by the regularization algorithm is further increased. Under the condition that the gray value error is +/−1, the spectral angle cosines of the spectral curves reconstructed by the regularization algorithm and by the Tsvd-Cvx algorithm are less than 0.972, and 100 random errors are applied, with a mean value less than 0.915. The spectral curve reconstructed by the regularization algorithm does not converge. From the above analysis, when the gray value error is +/−2, the accuracy of the spectral curve reconstructed by the regularization algorithm is poor and does not converge. The Tsvd-Cvx algorithm reconstructs the spectral curve with high accuracy and stability, achieving high-precision reconstruction.

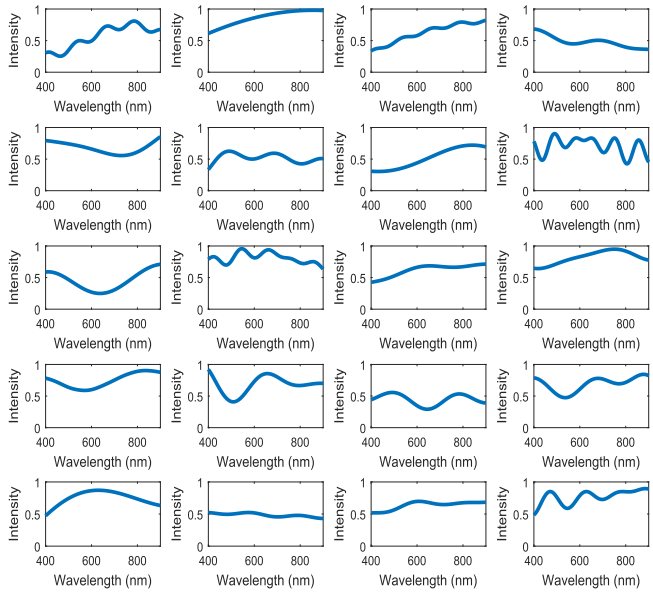

Fig. 12. Twenty $A(\lambda)$ curves.

VII. Conclusion

This paper analyzes three problems in micro-spectrometer engineering. First, due to the limited area of the photosensitive surface of the micro-spectrometer detector, this paper uses the K-means algorithm and particle swarm optimization to select the filter array based on 20 filter arrays. This approach reduces the number of conditions and satisfies the engineering requirements. Second, based on a combination of low-condition-number filters, this paper uses truncated singular value decomposition to determine the initial value and uses the solved initial value as a constraint on Cvx to solve the discrete value and perform fitting. This paper uses two target spectra as an example. Array B imposes a random error of plus or minus three gray values. Under these conditions, the spectrum is reconstructed. Third, this paper proposes a new evaluation method for spectral reconstruction curves, which uses multiple sets of reconstruction curves for cross-validation instead of relying on standard spectral curves to evaluate the spectrum. The results show that when the gray value error is $+/-2$, the cosine values of the spectral angles of two typical targets after cross-validation exceed 0.997 and 0.994, achieving high-precision reconstruction. To demonstrate the stability and accuracy of the Tsvd-Cvx algorithm, this paper compares the regularization algorithm with the Tsvd-Cvx algorithm for gray value errors of $+/-0.01$, $+/-0.1$ and $+/-1$. The results show that under 100 random errors, the cosine values of the spectral angles between the regularized reconstructed spectral curve and the Tsvd-Cvx algorithm reconstructed curve are less than 0.985, 0.981, and 0.915 for these error conditions, respectively. The accuracy of the spectral curve reconstructed by the regularized algorithm is lower than that of the Tsvd-Cvx algorithm. This method leads to a high-precision reconstruction and meets engineering requirements.

Disclosures: The authors declare no conflicts of interest.

Data availability: The data that supports the findings of this study are available within the article.

References

[1] J. Bao and M. G. Bawendi, "A colloidal quantum dot spectrometer," *Nature*, vol. 523, no. 7558, pp. 67–70, 2015.

[2] S. Zhang, Y. Dong, H. Fu, S.-L. Huang, and L. Zhang, "A spectral reconstruction algorithm of miniature spectrometer based on sparse optimization and dictionary learning," *Sensors*, vol. 18, no. 2, 2018, Art. no. 644.

[3] Y.-J. Wang et al., "Reconstruction simulation with quantum dots spectral imaging technology," *Spectrosc. Spectral Anal.*, vol. 38, no. 3, pp. 869–876, 2018.

[4] J. Oliver, W.-B. Lee, and H.-N. Lee, "Filters with random transmittance for improving resolution in filter-array-based spectrometers," *Opt. Exp.*, vol. 21, no. 4, pp. 3969–3989 2013.

[5] Y. Ma, Y. Zhang, and William W. Yu, "Near infrared emitting quantum dots: Synthesis, luminescence properties and applications," *J. Mater. Chem. C*, vol. 7, no. 44, pp. 13662–13679 2019.

[6] B. Liu et al., "Study on coaxiallinear dispersion triplet of wide spectral imaging spectrometer," *Spectrosc. Spectral Anal.*, vol. 36, no. 05, pp. 1543–1548, 2016.

[7] L.-H. Zheng, C.-H. Rao, N.-T. Gu, and Q. Qiu, "The aberration corrected spectrometer based on adaptive optics," *Spectrosc. Spectral Anal.*, vol. 36, no. 12, pp. 4088–4093, 2016.

[8] C.-C. Chang and H.-Y. Lin, "Spectrum reconstruction for on-chip spectrum sensor array using a novel blind nonuniformity correction method," *IEEE Sensors J.*, vol. 12, no. 8, pp. 2586–2592, Aug. 2012.

[9] C.-C. Chang, N.-T. Lin, U. Kurokawa, and B. I. Choi, "Spectrum reconstruction for filter-array spectrum sensor from sparse template selection," *Opt. Eng.*, vol. 50, no. 11, 2011, Art. no. 114402.

[10] U. Kurokawa, B. I. Choi, and C. Chang, "Filter-based miniature spectrometers: Spectrum reconstruction using adaptive regularization," *IEEE Sensors J.*, vol. 11, no. 7, pp. 1556–1563, Jul. 2011.

[11] L. Zhang, J.-K. Zhang, H.-Z. Song, W. Zhang, and W.-H Wang, "Case study on the fitting method of typical objects," *Photonics*, vol. 8, no. 10, 2021, Art. no. 432.

[12] L. Zhang, J.-K. Zhang, X.-Y. Lv, H.-Z. Song, and Wang W.-H, "Research on tunable spectrum reconstruction," *Spectrosc. Spectral Anal.*, vol. 42, no. 5, pp. 1378–1384, 2022.

[13] Y.-L. Ye, J.-Q. Zhang, D.-L. Liu, and Y.-X. Yang, "Research on a spectral reconstruction method with noise tolerance," *Curr. Opt. Photon.*, vol. 5, no. 5, pp. 562–575, 2021.

[14] L.-H. Zhang, D. Liang, D.-W. Zhang, X.-M. Gao, and X.-H. Ma, "Study of spectral reflectance reconstruction based on an algorithm for improved orthogonal matching pursuit," *J. Opt. Soc. Korea*, vol. 20, no. 4, pp. 515–523, 2016.

[15] J.-H. Zhang, X.-Y. Zhu, and J. Bao, "Solver-informed neural networks for spectrum reconstruction of colloidal quantum dot spectrometers," *Opt. Exp.*, vol. 28, no. 22, pp. 33656–33672, 2020.

[16] W.-H. Wang, X.-G. Luo, F.-Q. Wu, L. Lin, and J.-J. Li, "Spectral angles of plant leaves as indicators of uranium pollution in soil," *Spectrosc. Spectral Anal.*, vol. 42, no. 4, pp. 1313–1317, 2022.

[17] J.-B. Jin, D. You, G.-P. Wang, Z. Zhang, and Z.-C. Men, "Study on the detection of slight mechanical injuries on apples with hypersperspectral imaging," *Spectrosc. Spectral Anal.*, vol. 36, no. 7, pp. 2224–2228, 2016.

[18] P. Parrein, A. Landragin-Frassati, and J. M. Dinten, "Reconstruction method and optimal design of an interferometric spectrometer," *Appl. Spectrosc.*, vol. 63, no. 7, pp. 786–790, 2009.

[19] Y.-J Wang, J. Shen, L. Wei, Z.-H. Dou, and S.-S. Gao, "Inversion of photon correlation spectroscopy based on truncated singular value decomposition and cascadic multigrid technology," *Appl. Opt.*, vol. 52, no. 12, pp. 2792–2799, 2013.

[20] P. Gao et al., "Sparse view cone beam X-ray luminescence tomography based on truncated singular value decomposition," *Opt. Exp.*, vol. 26, no. 18, pp. 23233–23250, 2018.

[21] D.-S. Han, T. Liu, and Y.-C. Qi, "Optimization of mixed energy supply of IoT network based on matching game and convex optimization," *Appl. Opt.*, vol. 20, no. 19, pp. 5458–5458, 2020.

[22] B.-X. Gu, Y.-W. Chen, R.-X. Jiang, and X.-S. Liu, "Optimization of sparse cross array synthesis via perturbed convex optimization," *Sensors*, vol. 20, no. 17, 2020, Art. no. 4929.

[23] R. Chen and X. Li, "Implicit Runge-Kutta methods for accelerated unconstrained convex optimization," *IEEE Access*, vol. 8, pp. 28624–28634, 2020.